Journal of Magnetic Resonance 203 (2010) 57–65

Contents lists available at ScienceDirect

Journal of Magnetic Resonance

journal homepage: www.elsevier.com/locate/jmr

Cryogenic receive coil and low noise preamplifier for MRI at 0.01 T

Frank Resmer [a,b], Hugh C. Seton [a,*], James M.S. Hutchison [a]

[a] Bio-Medical Physics, University of Aberdeen, Foresterhill, Aberdeen AB25 2ZD, UK
[b] RAPID Biomedical GmbH, Rimpar, Germany

ARTICLE INFO

Article history:
Received 22 October 2009
Revised 30 November 2009
Available online 3 December 2009

Keywords:
Low field
Cooled
Litz
Low noise
Active damping

ABSTRACT

We have investigated the design and construction of liquid nitrogen cooled surface coils made from stranded (litz) copper wire for low field MRI applications. If designed correctly, cooled litz coils can provide a competitive alternative to high temperature superconducting (HTS) coils without the complications associated with flux trapping. Litz coils can also be produced with a wider range of shapes and sizes, and at lower cost. Existing models were verified experimentally for flat spiral coils wound from solid and litz wires, operated at room temperature and 77 K, and then used to design and optimise a cooled receive coil for MRI at 0.01 T (425 kHz). The *Q*-factor reached 1022 when the coil was cooled to 77 K, giving a bandwidth of just 0.42 kHz, so a low noise JFET preamplifier was developed to provide active damping of the coil resonance and thus minimise image intensity artefacts. The noise contribution of the preamplifier was determined using a method based on resistive sources and image noise analysis. The voltage and current noise were measured to be 1.25 nV/ $Hz^{1/2}$ and 51 fA/ $Hz^{1/2}$, respectively, and these values were used to estimate a noise figure of 0.32 dB at the resonant frequency of the cooled coil. The coil was used to acquire 0.01 T spin echo images, first at room temperature and then cooled to 77 K in a low noise liquid nitrogen cryostat. The measured SNR improvement on cooling, by a factor of 3.0, was found to correspond well with theoretical predictions.

1. Introduction

Low field magnetic resonance imaging (MRI) suffers from low signal levels compared to high field [1], but has the advantages of reduced hardware and installation costs and also offers the possibility of enhanced T_1 contrast between tissues [2]. The signal to noise ratio (SNR) at low field can be improved by averaging, but only at the expense of increased acquisition times.

The SNR at low field can also be increased by cooling the radio-frequency (RF) coil and reducing its resistance. In a well-designed MRI system the SNR is determined by Johnson noise from the sample and receive coil. At low field strengths sample noise is usually less than that from the receive coil [1], particularly if a surface coil is used [3]. A coil with a frequency dependent resistance, $R(f)$, generates a noise voltage, V_s, with an RMS value of:

$$V_s = \sqrt{4k_B TR(f)\Delta f} \tag{1}$$

where k_B is Boltzmann's constant, T the coil temperature and Δf the measurement bandwidth. $R(f)$ may be estimated from the coil's inductance, L, and Q-factor using:

$$Q = \frac{2\pi fL}{R(f)} \tag{2}$$

Early work on cooled coils for MRI used solid copper conductors cooled with liquid nitrogen [4] but interest then moved to the development of high temperature superconducting (HTS) receive coils. Many research groups have described HTS coils with *Q*-factors of several thousand at liquid nitrogen temperature (77 K) and below, which yield SNR improvements, relative to room temperature coils, of between 1.5 and 10 times (e.g. [5–11]). HTS coils, however, are susceptible to flux trapping so that the working *Q*-factor in an MRI scanner's main magnetic field may be considerably lower than measured in the open laboratory [5,11]. HTS coils exhibiting the lowest losses have been fabricated using thin-film patterning, with tuning capacitors incorporated as part of the coil windings [7,11]. This method tends to limit the size, shape and tuning flexibility, as well as increasing the cost of HTS coils. HTS materials also tend to degrade with thermal cycling, due to mechanical stresses and changes in chemical composition caused by moisture formation, but reliability can be improved by mechanical cooling, rather than immersion in liquid nitrogen [9,11].

One way to reduce resistive losses in room temperature receive coils for low field MRI is to use stranded copper (litz) windings [12–14]. This article describes the development of a litz wire surface coil cooled with liquid nitrogen. Although the intrinsic losses from this approach are higher than in HTS materials, a properly

* Corresponding author.
E-mail address: h.seton@abdn.ac.uk (H.C. Seton).

1090-7807/$ - see front matter © 2009 Elsevier Inc. All rights reserved.
doi:10.1016/j.jmr.2009.11.021

designed, cooled litz coil will out-perform a cooled solid copper winding at low field strengths, and will not suffer any Q-factor reduction when placed in the main imaging field. Litz coils can also be produced in almost any shape and size and at much lower cost than HTS equivalents.

2. Theory

The following sections outline the theory required to design litz surface coils for use at room temperature and 77 K, and also special preamplifiers, incorporating active damping, which help to prevent image intensity artefacts without adding noise.

2.1. Litz wire

The effective resistance of a wire of resistivity, ρ, at a frequency, f, is greater than its DC value because the current flow is effectively restricted to a thin surface layer, given by the skin depth, δ, where [15]:

$$\delta = \sqrt{\frac{\rho}{\pi f \mu_0}} \tag{3}$$

Fig. 1(a) shows a solid wire of diameter d_0, much greater than δ, for which the effective area available to carry RF current, A_{eff}, is:

$$A_{\text{eff}} = \pi d_0 \delta \quad (d_0 \gg \delta) \tag{4}$$

Given that a conductor's resistance is inversely proportional to A_{eff}, Eqs. (3) and (4) show that the RF resistance of a solid wire, for which $d_0 \gg \delta$, scales with $f^{1/2}$. Litz wire, by contrast, comprises a large number, N_s, of insulated strands of diameter, d_s, twisted together. Fig. 1(b) shows how this construction can increase A_{eff} if the strand radius is small compared to the skin depth at the operating frequency, to a value of:

$$A_{\text{eff}} = N_s \frac{\pi d_s^2 \delta}{4} \quad (d_s \ll \delta) \tag{5}$$

Although skin effect losses are reduced in litz wire, the tight packing of strands causes eddy current (proximity effect) losses, which depend on the thicknesses of the copper conductor and insulation in each strand, on the number of strands in the wire and which scale with f^2 [15]. Litz wire contains more insulating material than solid wire of the same outer diameter, so the DC resistance is greater, and this is further increased because each twisted strand is longer than the completed wire.

There is also a proximity effect due to eddy currents between neighbouring turns. For solid copper wire, the Q-factor is optimised with an inter-turn spacing approximately equal to the wire diameter [16]. Litz wire's structure greatly reduces the inter-turn proximity effect, so litz wire turns may be placed closer together, increasing the coil inductance without any significant increase in proximity losses and, from Eq. (2), further increasing the Q-factor.

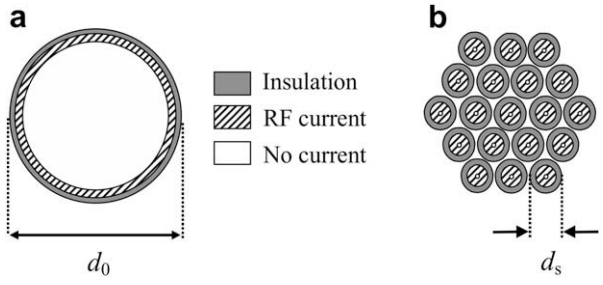

Fig. 1. Effective cross-sectional areas for RF currents, A_{eff}, of (a) solid copper wire of diameter d_0 and (b) litz wire composed of N_s individual strands, each of diameter d_s. For each wire the skin depth is δ.

Losses in any copper coil may be reduced by cooling. The resistivity of copper reduces by a factor of 8 on cooling with liquid nitrogen to 77 K [17] but Eq. (3) shows that this is accompanied by a reduction in skin depth which at 425 kHz, the proton resonance frequency at 0.01 T, falls from 100 μm (300 K) to 35 μm (77 K). As a result A_{eff} for a solid wire, given by Eq. (4), is reduced by approximately the same factor (2.8), so the AC resistance only reduces by a factor of 8/2.8, or 2.8 times. The performance of litz-wound coils can be improved by cooling but, for this to be effective, the litz strand radius should be less than the skin depth at 77 K (35 μm), so that the current density at the centre of the strand is not significantly smaller than that at the strand surface.

We have developed a flat, circular spiral (pancake) coil for use at 0.01 T. During the design process we compared the performance of solid and litz windings at 300 K and 77 K. Each type is affected by AC loss contributions from the skin effect, the proximity effect between turns and, for the litz coil, the proximity effect between strands within each turn. The resistance ratio, F, between a coil's AC and DC resistances can be expressed as:

$$F = \frac{R_{\text{AC}}}{R_{\text{DC}}} = H + \lambda G \tag{6}$$

where H and G are frequency-dependent skin effect and proximity effect factors [18], and λ is a factor accounting for the particular coil geometry.

Using tabulated data, F may be calculated for a variety of coil shapes, wound from solid and litz wire [15,18]. For a single layer pancake coil of outer diameter, D, wound with m turns of solid wire of diameter d_0, the resistance ratio is:

$$F = H + \frac{1}{4}\left(\frac{K d_0^2 m}{cD}\right)^2 G \tag{7}$$

where K is a constant depending on the coil geometry and c is the centre-to-centre turns spacing [15].

For a single layer pancake coil wound from litz wire the resistance ratio is given by:

$$F = H + \left[k + \frac{1}{4}\left(\frac{K d_0^2 m}{cD}\right)^2\right]\left(\frac{d_S}{d_0}\right)^2 n^2 G \tag{8}$$

where n is the number of strands, each of diameter d_S and k is a constant depending on n [15]. Eq. (8) indicates that proximity losses can be reduced by reducing the number and diameter of litz strands. However, this will also increase the DC resistance, so a compromise must be found.

As well as the magnetic effects described above, it is also necessary to account for the stray capacitance between the coil's turns, and the effect of dielectric losses in the materials used for the wire's insulation and the coil's substrate. Dielectric losses can be modelled as an additional series resistance, R_e, of the form:

$$R_e = \tau f^3 L^2 C_d \tag{9}$$

where τ is the loss factor of the material, L the coil's inductance and C_d the distributed lossy capacitance [1,15]. Although the f^3 dependence indicates that dielectric losses are most significant at high frequencies, they can also limit the Q-factor of litz wire coils below 1 MHz. In practice R_e may be estimated for a given type of coil construction from the Q-factor at the coil's self-resonance, and then this value scaled with frequency using Eq. (9).

2.2. Low noise preamplifiers and active damping

The Johnson noise produced by a cooled coil is so small that ultra-low noise preamplifiers are needed to preserve the SNR [19–21]. At high field strengths RF coils are commonly matched to standard coaxial cables and connected to 50 Ω preamplifiers to minimise reflections and signal loss [16], although deliberate mismatching is used in phased arrays [22] where coil interactions are reduced in exchange for some increase in preamplifier noise factor. By contrast, at the 425 kHz operating frequency of the MRI system used for this work, all paths within the RF receiver are much shorter than a quarter wavelength and so it is possible to connect a parallel-tuned RF coil directly to the input of a high impedance preamplifier without sacrificing noise factor [19–21].

Preamplifier noise performance can be described by independent voltage and current noise generators, V_n and I_n [23]. The total output noise, V_{out}, from a preamplifier with a parallel resonant coil connected to its input is given by:

$$V_{out} = A\sqrt{V_s^2 + V_n^2 + (ZI_n)^2} \tag{10}$$

where A is the preamplifier's gain, Z is the receive coil's parallel impedance and V_s is the source voltage noise, given by Eq. (1), due to the resistive part of Z [23].

The preamplifier's noise factor, N, is given by:

$$N = 1 + \frac{V_n^2 + (ZI_n)^2}{V_s^2} \tag{11}$$

and is used to evaluate the amount by which the preamplifier degrades the coil's SNR [23]. The optimum source impedance of the preamplifier, at which N is a minimum, is given by V_n/I_n so ideally the RF coil's impedance should be close to this value. As the cooled litz coil described in this article is operated in parallel resonance and connected directly to the preamplifier input its effective impedance at resonance is given by [15]:

$$R_d \approx \omega LQ \tag{12}$$

In an optimised, tuned system the preamplifier's noise factor, N, has a minimum at the coil's resonance but degrades at higher and lower frequencies as the coil's parallel impedance decreases, which can lead to SNR variations across the frequency encoding axis of an image.

Apart from SNR variations, frequency-encoded MRI acquisitions can also display intensity artefacts if the coil's 3 dB bandwidth, Δf, is less than the image acquisition bandwidth [20]:

$$\Delta f = \frac{f_0}{Q} \tag{13}$$

where f_0 is the resonant frequency. The 425 kHz MRI system uses an acquisition bandwidth of 5 kHz so Eq. (13) indicates that Q-factors exceeding 85 would cause unacceptable variations in image intensity. It would be possible to increase Δf by adding resistance, but only at the expense of extra noise.

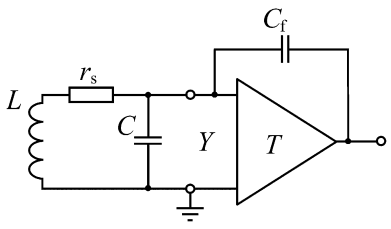

Fig. 2. A receiver circuit with active damping.

Fig. 2 shows a better scheme, in which part of the inverted signal from the preamplifier output is fed back to the coil, resulting in active damping of the coil resonance [19–21,24]. As long as the feedback path generates no noise (here it is the capacitor C_f) the intrinsic amplifier noise should not be increased [24]. A suitable preamplifier has a transfer function, $T(\omega)$, with an integrating characteristic described by:

$$T(\omega) = \frac{j}{\omega\tau} \tag{14}$$

where τ is the integrating time constant and ω the angular frequency. The effective input admittance, Y_{in}, is found to be:

$$Y_{in} = j\omega C_f + \frac{C_f}{\tau} \tag{15}$$

Provided the time constant is chosen so that $\tau \gg 1/\omega$, it can be shown that the feedback circuit simulates a noiseless resistor, τ/C_f, in parallel with the preamplifier input. This damps the coil by effectively shunting the dynamic resistance, R_d, given by Eq. (11).

3. Methods and materials

3.1. Cooled litz coil and solid wire evaluation coil

A litz surface coil was constructed for use in a horizontal field, 0.01 T MRI system. As already stated, the litz strand diameter should be comparable to the skin depth to ensure a low AC resistance. The strands should not be made much thinner than this though, because then the DC resistance of a litz wire of given outer diameter would be increased by having a larger proportion of the cross-section filled by strand insulation material rather than copper (Fig. 1(b)). The skin depth of copper at 425 kHz (the proton resonance frequency at 0.01 T) is 35 μm at 77 K, so Litz wire was selected from a commercial supplier [25] with 600 polyurethane-insulated, copper strands of 30 μm diameter. A single layer, close packed spiral coil (pancake coil) of this wire, with 21 turns of inner and outer diameters 55 mm and 113 mm, was fixed to the 5 mm-thick base of a G10 fibreglass cryostat (described in the next section) using cyanoacrylate adhesive. A second pancake coil with similar dimensions was constructed from solid copper wire to allow measurements on equivalent solid and litz coils at 300 K and 77 K to test the theory outlined in Section 2.1. The solid coil was wound from 19 turns of 1 mm diameter copper wire with inner and outer diameters of 55 mm and 120 mm and an inter-turn spacing of approximately 0.9 mm to reduce proximity effect losses [16]. The solid coil was also fixed to a 5 mm-thick G10 fibreglass substrate with cyanoacrylate adhesive to give similar dielectric losses to the litz coil.

Each coil's 4-terminal DC resistance was measured first at room temperature and then immersed in liquid nitrogen (at 77 K), by feeding with a constant current from a stabilised power supply (EX354D, Thurlby-Thandar Instruments Ltd., UK) and measuring the voltage drop. Next, the coils were tuned over a range of frequencies from 130 kHz to 6 MHz using standard polystyrene capacitors (LCR Capacitors Ltd., UK). Q-factors were recorded, again at both temperatures, by placing the coils between 1 cm diameter wire loops, one driven by a variable frequency RF source (33120A, Hewlett Packard) and the other connected to a high impedance preamplifier and oscilloscope. The Q-factors were determined, using Eq. (13), from the 3 dB points of the recorded resonance curves, taking care that the drive and pick-up loops did not load the coils under test, and coil inductances were calculated from the resonant frequency and capacitance value. The frequencies and Q-factors of the solid and litz coil's self-resonances, without additional tuning capacitance, were also recorded to allow the contribution from dielectric losses to be assessed.

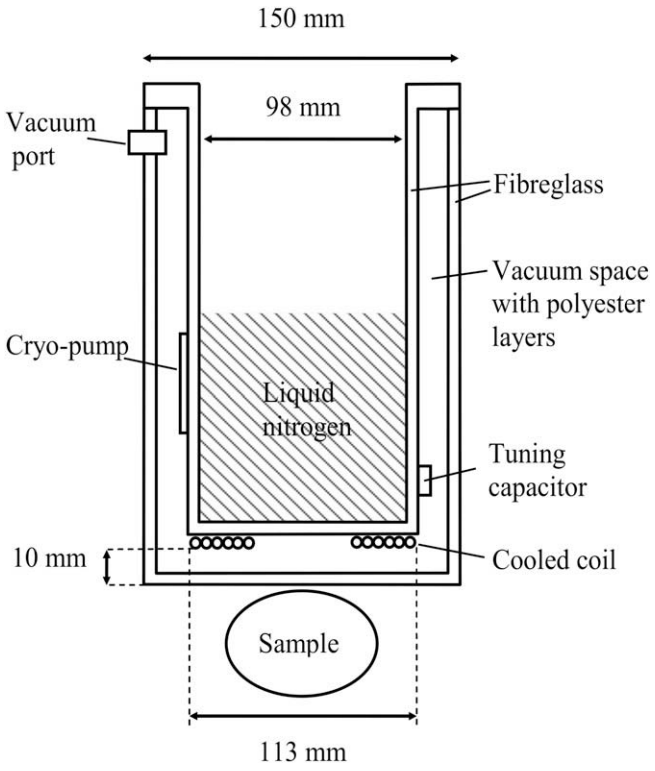

Fig. 3. The conduction-cooled receiver coil and fibreglass liquid nitrogen cryostat.

3.2. Liquid nitrogen cryostat

During imaging the litz coil is cooled with a liquid nitrogen cryostat made from G10 fibreglass, with a 2.5 L liquid capacity (Fig. 3). The coil is fixed to the lower face of the liquid nitrogen reservoir in the vacuum space, and so is cooled by conduction rather than direct immersion in liquid nitrogen. Mounting the coil like this increases the maximum outer winding diameter from the 98 mm available in the liquid reservoir to 113 mm and also reduces the coil-sample spacing from 17 mm to 10 mm when cooled, both of which help to improve magnetic coupling with the sample. The cryostat is evacuated to a base pressure below 0.02 mbar, and the pressure is further reduced by a charcoal cryo-pump fitted around the reservoir, which becomes active once the cryostat is filled [17]. In addition, approximately 10 layers of polyester fabric are wrapped around the reservoir to prevent residual gas molecules from transferring energy directly from the 300 K outer cryostat wall to the coil.

Before imaging, the temperature achieved with conduction cooling was compared with the value from direct immersion in liquid nitrogen at 77 K, using 4-terminal DC resistance measurements of the winding. After the liquid reservoir was filled the conduction cooled resistance fell approximately exponentially with time towards the direct immersion value until, after about 20 min, the resistances were identical, indicating that conduction cooling had successfully achieved a base temperature of 77 K.

The coil is parallel-tuned using polystyrene capacitors with a combined value of 2.8 nF (LCR Capacitors Ltd., UK), mounted close to the windings in the vacuum space to minimise losses. The signal is carried to a vacuum feed-through at the top of the cryostat via a pair of litz signal leads in good thermal contact with the liquid nitrogen reservoir, and then to the room temperature FET preamplifier. The litz coil's 425 kHz Q-factor was recorded at 300 K and 77 K once the cryostat and leads were assembled, using the method described above for the isolated coils.

3.3. JFET preamplifier and noise measurement

When cooled, the litz coil's bandwidth is well below the MRI system's imaging bandwidth of 5 kHz and, if uncorrected, this mismatch would result in unacceptable image intensity variations across the frequency encoding direction. Fig. 4 shows a high input impedance preamplifier which uses the principles described in Section 2.2 to provide active damping of the coil's resonance. The input stage (Q1) is a J309 Junction Field Effect Transistor (JFET) [26]. Transistors Q2 and Q3 provide a trans-impedance stage with an integrating characteristic defined by C_i. The active damping signal is fed back to the coil via C_f, as described in Section 2.2, and Q4 buffers the output.

Fig. 5 shows an equivalent noise model of a resistive source connected to this preamplifier [23]. As long as noise from the source and preamplifier dominates that from all subsequent stages in the MRI receiver electronics, the preamplifier's voltage noise, V_n, can be determined by shorting the input and measuring V_{out} from an image. However, using this method it would be necessary to know the system gain, A_{sys}, to relate the image noise to the preamplifier's input voltage noise. An alternative method is to measure the RMS image noise for a range of source resistances, R_s, with a maximum value small enough that the noise contribution (in Eq. (10)) from V_n always dominates that from I_n.

The usual way to determine current noise, I_n, is to measure the equivalent open-circuit voltage noise, V_{open} (i.e. with an open cir-

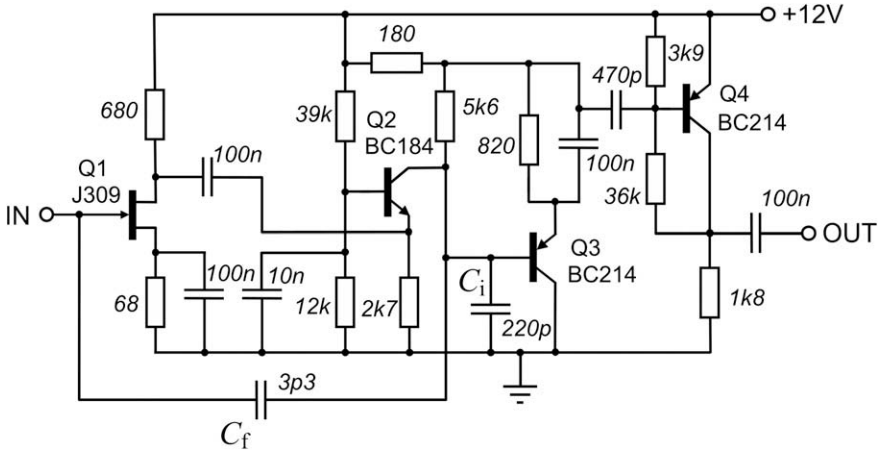

Fig. 4. The high input impedance preamplifier, with active damping from the feedback capacitance C_f.

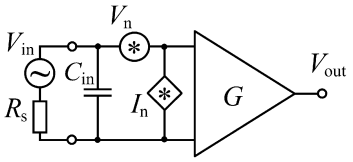

Fig. 5. Noise model of the JFET preamplifier.

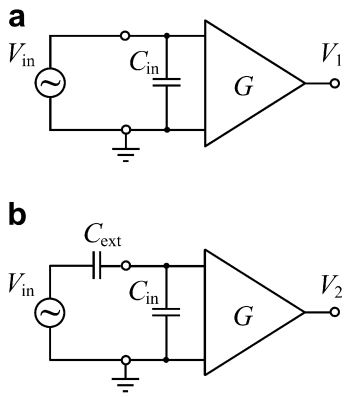

Fig. 6. Measurement of the preamplifier's input capacitance using a signal generator connected (a) directly to input and (b) via capacitance C_{ext}.

cuit at the input). However in practice the input capacitance of the first stage, C_{in}, shown in Fig. 5 effectively shunts the source resistance, R_s, at high frequencies and has to be considered as part of the source impedance, Z, for noise measurements so that:

$$Z = \frac{R}{1 + j\omega C_{in} R} \tag{16}$$

where ω is the angular frequency. C_{in} can be estimated using the method shown in Fig. 6. Firstly a signal generator is connected directly to the preamplifier input and the output voltage, V_1, recorded (Fig. 6(a)). Then a known capacitor, C_{ext}, is connected in series with the input (Fig. 6(b)) to form a potential divider with C_{in}, so that a reduced output voltage, V_2, is measured. C_{in} is then calculated using:

$$C_{in} = C_{ext}\left(\frac{V_1}{V_2} - 1\right) \tag{17}$$

Once C_{in} is known, Eqs. (10) and (16) allow I_n to be deduced from measured values of V_{open} and V_n. It is not possible to measure V_{open} directly because the preamplifier requires a certain shunt resistance to supply bias current to the JFET gate. However, an estimation can made by plotting the mean-squared image noise versus source conductance, $G = 1/R$. In contrast to the determination of V_n described above, the source resistances, R, used to measure current noise need to be sufficiently large to yield measurable noise contributions from I_n in Eq. (10).

Table 1
Inductances, DC resistances and self-resonance characteristics of pancake coils wound from solid and litz wire at 300 K and 77 K.

	Solid coil	Litz coil
Number of turns	19	21
Inner/outer diameter (mm)	55/120	55/120
Inductance (μH)	36	46
R_{DC} at 300 K (mΩ)	146	251
R_{DC} at 77 K (mΩ)	17.7	31
Self-resonance, f_s (MHz)	13.1	8
Q-factor at f_s and 300 K	81	61
Q-factor at f_s and 77 K	561	153

4. Results

The frequency dependence of the solid and litz coils' Q-factors were recorded at 300 K and 77 K and the JFET preamplifier's noise contributions were measured. The cooled litz coil and preamplifier were then used to acquire low field magnetic resonance images.

4.1. Q-factors of solid and litz coils at 300 K and 77 K

Eq. (7) was used with tabulated data [15] to calculate the resistance ratios, F, for the solid-wire coil between 100 kHz and 10 MHz at both 300 K and 77 K. These values, and the coil's actual DC resistance and inductance recorded in Table 1, were used to calculate the Q-factor over the same frequency range and at both temperatures. The results of this simulation are shown in Fig. 7 together with data measured from the solid-wire coil. Likewise, Eq. (8) was used to predict the frequency dependence of the Q-factor for the litz wire pancake coil at both temperatures, and the simulated and measured data are shown in Fig. 8.

Losses in the solid-wire coil are dominated by the skin effect at low frequencies, so that the Q-values shown in Fig. 7 increase with $f^{1/2}$ as indicated by Eqs. (3) and (4). The measured points for the solid coil are in reasonable agreement with the simulation at low frequencies but begin to deviate as the coil's self-resonance is approached. However, once dielectric losses are included in the simulation, using values deduced from the Q-factors at self-resonance, f_s, shown in Table 1 and the f^3 dependence predicted by

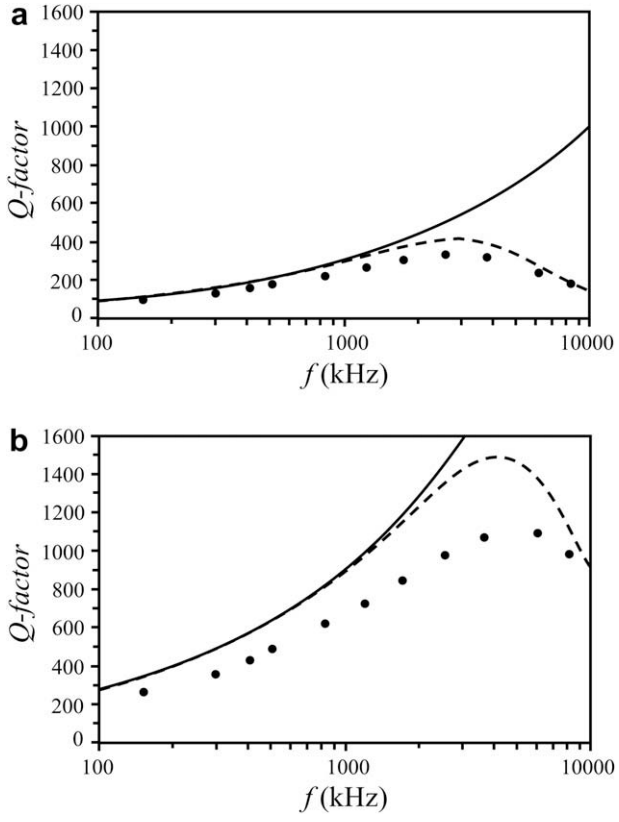

Fig. 7. Q-factors of a 120 mm diameter, 19 turn solid wire pancake coil at (a) room temperature and (b) 77 K showing simulated curves without (continuous) and with (dashed) dielectric losses, and the measured points.

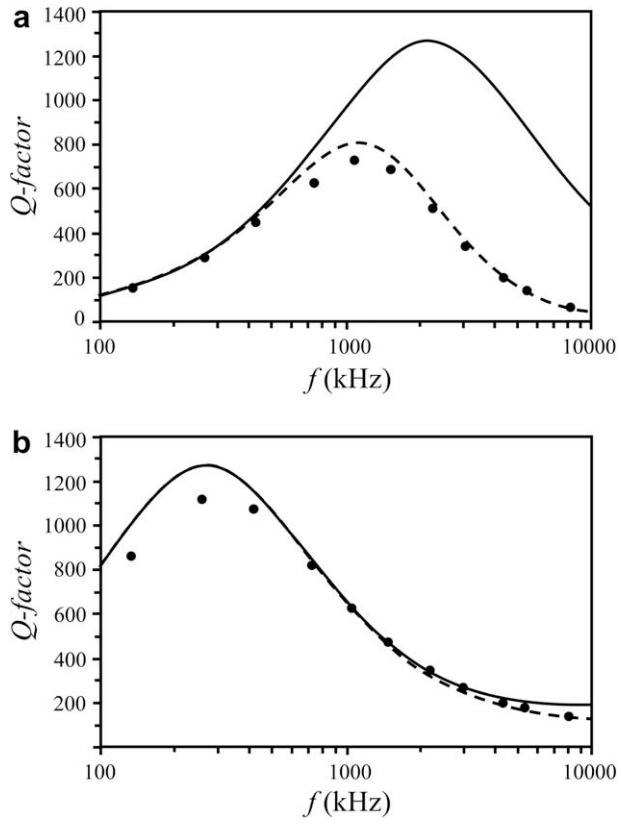

Fig. 8. *Q*-factors of a 113 mm diameter, 21 turn litz wire pancake coil at (a) room temperature and (b) 77 K showing simulated curves without (continuous) and with (dashed) dielectric losses, and the measured points.

Eq. (9), there is much better agreement with the real data so that the model correctly predicts *Q*-factor maxima at approximately 2.5 MHz when used at 300 K (Fig. 7(a)) and 4 MHz at 77 K (Fig. 7(b)).

The simulations of the litz coil without dielectric losses (Fig. 8 continuous curves) predict *Q*-factor maxima of 1270 at 2.5 MHz when used at 300 K (Fig. 8(a)) and of 1270 at 300 kHz when used at 77 K (Fig. 8(b)), which arise from the different frequency dependences of the skin and proximity effects described in Section 2.1. The real data differs from the simulation at room temperature, with a maximum *Q*-factor of 730 at 1.1 MHz, but shows similar behaviour to the simulation when cooled to 77 K, with a maximum cooled *Q*-factor of 1100 at about 300 kHz. Once dielectric losses are included (dashed curves in Fig. 8) there is much better agreement between simulation and measurement for the litz coil at room temperature, with a maximum predicted *Q*-factor of 820 at 1.1 MHz, and the model correctly predicts that when the coil is cooled, dielectric losses have a negligible effect on *Q*-factor at the intended 425 kHz operating frequency.

In a well-designed litz coil without dielectric losses, DC losses exceed the skin effect at low frequencies, so the *Q*-factor, given by Eq. (2), scales with f. The *Q*-factor increases until proximity effects within the wire, which scale as f^2, equal the DC losses, corresponding to $F = 2$ in Eq. (6). Above the maximum the *Q*-factor scales approximately as $1/f$. The continuous curves in Fig. 8(a) and (b) show that cooling the litz coil does not change the maximum achievable *Q*-factor from the room temperature maximum, but reduces the optimum frequency by approximately the same factor as the reduction in the conductor's resistivity. The dashed curves show that when dielectric losses are included, both the value and frequency of the maximum *Q*-factor possible with this type of litz pancake coil are reduced at room temperature, but there is little change in the behaviour when the coil is cooled.

The "working" *Q*-factors for the litz coil at 425 kHz, in the fully assembled cryostat with signal leads attached, were 425 at 300 K and 1022 at 77 K. These values are slightly lower than those for the isolated coil shown in Fig. 8 (446 and 1070, respectively), presumably as a result of losses in the signal leads and vacuum feedthrough. The working values are used in the following sections to estimate the preamplifier's noise factor and the expected SNR gains when the coil is cooled.

4.2. Preamplifier's voltage noise, current noise and time constant

As described in Section 3.3, provided that the preamplifier is the dominant noise source in the imaging system, its voltage and current noise contributions can be estimated from images acquired with fixed resistors in place of the RF coil. For these measurements noise data, demodulated at 425 kHz by the MRI receiver electronics, were sampled with 12-bit resolution at 128 points using a 5 kHz readout bandwidth and with 128 repetitions. Data were converted to 128 × 128 pixel noise images using a standard 2D FT routine, with an effective pixel noise bandwidth of 0.305 Hz, found by dividing the readout bandwidth by the total number of pixels. Average pixel intensities, P, of the resulting noise images were recorded in units of the least significant bit (LSB) from centrally placed regions of interest.

The preamplifier's voltage noise, V_n, and the system gain, A_{sys}, were determined by plotting the mean-squared image noise, P^2, against R for five resistance values between 91 Ω and 2 kΩ, as shown in Fig. 9. The fitted line shows good agreement with the points ($r^2 > 0.999$) and intercepts the x axis at $R = -95$ Ω which can be thought of as the "negative" resistance which would compensate for the noise contribution from the preamplifier. Eq. (1) shows that an equivalent noise resistance of 95 Ω would produce a Johnson voltage noise with an RMS value of 1.25 nV/Hz$^{1/2}$, and this is taken to be the amplifier voltage noise V_n. The overall system gain, A_{sys}, can now be estimated from the y-intercept value of 85 LSB^2, which is the image (output) noise that would result from a shorted input. Dividing by the pixel bandwidth of 0.305 Hz yields a normalised image noise intensity of 16.7 LSB/Hz$^{1/2}$ and this is then divided by V_n, calculated above, to give a value for A_{sys} of 13.4 LSB/nV.

The current noise, I_n, was estimated by plotting the mean-squared image noise, P^2, versus source conductance, $G = 1/R$, for source resistances between 91 kΩ and 1 MΩ. Fig. 10 plots the re-

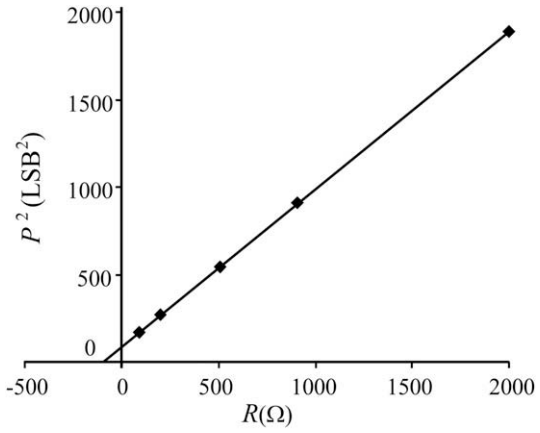

Fig. 9. Graph of mean square pixel intensity versus source resistance from images recorded at 0.305 Hz pixel bandwidth, used to determine the JFET preamplifier's voltage noise.

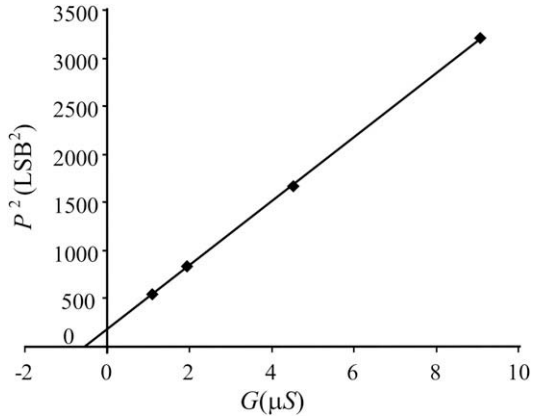

Fig. 10. Graph of mean square pixel intensity versus source conductance from images recorded at 0.305 Hz pixel bandwidth, used to determine the JFET preamplifier's open-circuit noise.

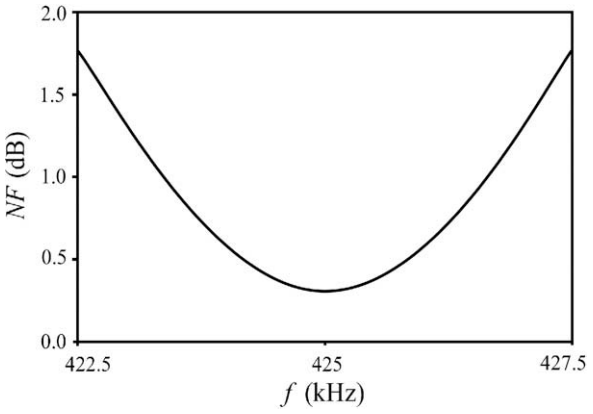

Fig. 11. Simulated frequency dependence of the preamplifier's noise figure for the cooled litz coil.

sults and, again, the fitted line shows good agreement with the measured points ($r^2 > 0.999$). The y-intercept in Fig. 10, of 177 LSB^2, corresponds to the output noise at 425 kHz with an open-circuited input. Dividing by the pixel bandwidth gives a normalised image noise intensity of 24.1 LSB/Hz$^{1/2}$ and then division by A_{sys} estimates that the open-circuit noise referred to the preamplifier's input, V_{open}, is 1.8 nV/Hz$^{1/2}$. The preamplifier's input capacitance, C_{in}, was estimated using the method shown in Fig. 6 and Eq. (17) gives a value of 15 pF ± 0.8 pF, with the uncertainty governed by the 5% tolerance of C_{ext}. Eq. (16) is used to estimate an input impedance $|Z_{in}| = 1/\omega C_{in}$ of 25 ± 1.3 kΩ at 425 kHz which, in turn, allows I_n to be calculated from V_{open} and V_n. It is not known to what extent V_n and I_n in Eq. (10) are correlated. Completely correlated sources would give $I_n = (V_{open} - V_n)/Z_{in}$ while, for un-correlated sources the result would be $I_n = (V_{open}^2 - V_n^2)^{1/2}/Z_{in}$ [20]. For this reason I_n is estimated to lie somewhere between 22 fA/Hz$^{1/2}$ and 51 fA/Hz$^{1/2}$. The amplifier's optimum source impedance, for which its noise figure is minimum, equals V_n/I_n and so lies somewhere between 24 kΩ and 57 kΩ.

The integrating time constant, τ, of the preamplifier shown in Fig. 4 was calculated from Eq. (14) by measuring the magnitude of the transfer function, $|T(\omega)|$, between the gate of Q1 and the collector of Q2 but without a feedback capacitor, C_f, connected. The measurement was repeated for a range of frequencies between 200 kHz and 1 MHz and then $1/|T(\omega)|$ was plotted against ω. The gradient of the fitted straight line through this graph gave a value for τ of 31 ns. The phase shift between these points in the circuit was +90° over the range of frequencies tested, in agreement with the constant phase shift predicted by Eq. (14).

4.3. Preamplifier's noise figure with the cooled litz coil

Eq. (12), the data in Table 1 and the working Q-factor of 1022 at 77 K predict that when cooled, the litz coil has a dynamic resistance, R_d, of about 120 kΩ at resonance. The preamplifier's noise figure, NF, is then estimated to lie between 0.07 dB and 0.32 dB ($NF = \log_{10}(N)$ where N is given by Eq. (11)) depending on the actual current noise level. To see how the noise figure degrades away from resonance, the coil's frequency response is assumed to fit a Lorentzian. Then the magnitude of the coil's parallel impedance, used to calculate the current noise contribution in Eq. (10), reduces from 120 kΩ at resonance to approximately 10 kΩ at the edges of the 5 kHz imaging bandwidth, whereas the real part of the impedance, used to calculate the source noise in Eq. (10), reduces from 120 kΩ to 830 Ω at the edges. Fig. 11 simulates the frequency dependence of the preamplifier's noise figure, assuming the highest estimated current noise value of 51 fA/Hz$^{1/2}$, when coupled to a coil with parameters given in Table 1 and a working Q-factor of 1022 at 77 K. It is seen that the noise figure rises from a minimum of 0.32 dB at resonance to 1.8 dB at the edges of the image.

4.4. Low field MRI with the cooled litz coil

Imaging experiments were carried out in a horizontal field, 0.01 T MRI system based on a resistive, Helmholtz magnet. The transmit field was generated by a 30 turn, 7 cm long, 24 cm diameter saddle coil with a Q-factor of 25. The coil was driven by a 10 W, gated MOSFET amplifier and passive decoupling diodes were used to prevent noise currents during signal acquisition.

The un-damped litz receiver coil exhibits Q-factors of 425 at 300 K and 1022 at 77 K, with associated bandwidths of just 1 kHz and 0.42 kHz, respectively, both significantly below the MRI system's 5 kHz acquisition bandwidth. Therefore a damping capacitance, C_f, was added to the preamplifier, as shown in Fig. 4, calculated to give a damped bandwidth of approximately 6 kHz and a corresponding Q-factor of 70 at both temperatures. Eq. (12) shows that the coil's dynamic resistance at resonance, R_d, would then equal about 8.5 kΩ compared to its un-damped values of 51 kΩ at 300 K and 120 kΩ at 77 K. This reduction requires an additional resistance of approximately 9.5 kΩ in parallel with the coil. Eq. (15) shows that the feedback preamplifier generates an equivalent damping resistance equal to τ/C_f so, from the measured τ of 31 ns it follows that a damping capacitance of about 3.2 pF is required. In practice the nearest available value, 3.3 pF, was used for both temperatures, and damped Q-factors were measured of 68 at 300 K and 73 at 77 K, in close agreement with the intended value of 70.

First a pair or images were acquired to measure the SNR improvement on cooling. A phantom comprising a 3 × 3 array of 25 mm diameter plastic bottles filled with $CuSO_4$ solution (T_1 = 45 ms and T_2 = 44 ms) was positioned directly below the cryostat base. Fig. 12 shows transaxial spin echo images, accumulated from 16 averages, (a) with the receive coil at room temperature and (b) with it cooled in liquid nitrogen. SNR values for each image were calculated by measuring the ratio of pixel intensities between a region in the centre bottle in the top row and a background noise region below the bottom row of bottles, and applying the accepted correction factor [27]. The SNR of the coil was found to be 11.4 at 300 K and 34.0 when cooled to 77 K. Fig. 13 shows a coronal spin echo image of a volunteer's palm acquired with the cooled litz coil, in which the bones are clearly resolved. During acquisition the base of the cryostat was initially cool to the touch,

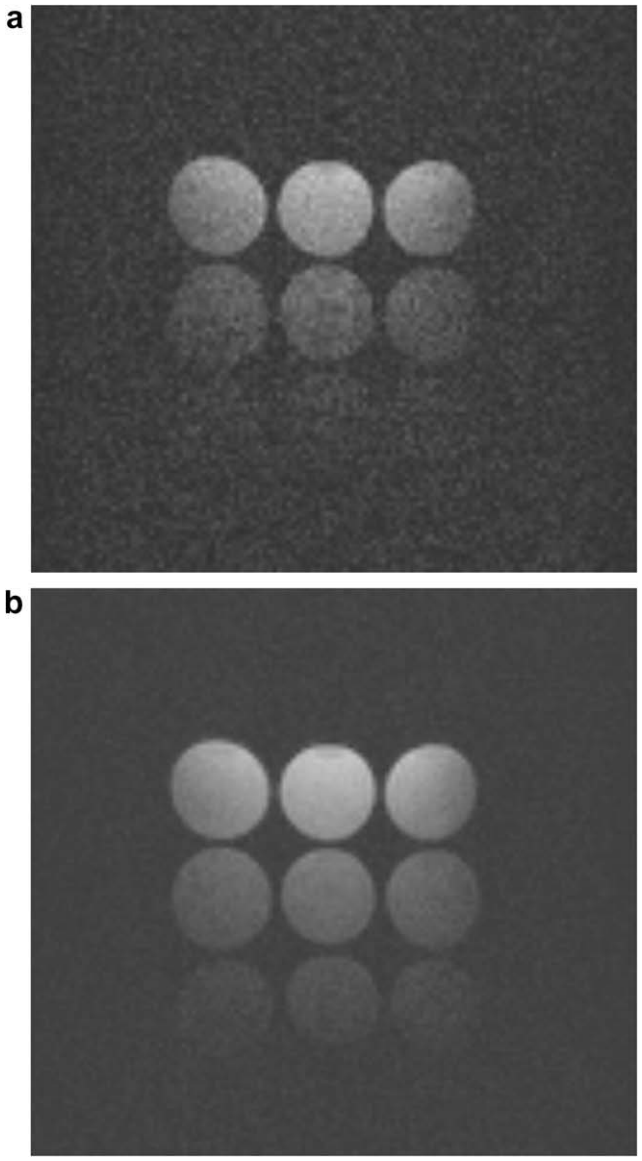

Fig. 12. Transaxial spin echo images of a bottle phantom acquired at 0.01 T with the litz receive coil (a) at room temperature and (b) cooled to 77 K (TE = 20 ms, TR = 200 ms, 128 pixel^2, 16 averages, FOV = 15 cm, slice thickness = 2 cm).

but soon warmed up to body temperature, confirming that there was a low heat leak across the 10 mm coil-sample separation.

5. Discussion and conclusion

Measurements of phantom images acquired with the litz coil at 300 K and 77 K show that the SNR in the centre of the top row of imaged bottles increases by 3.0 when the coil is cooled. The SNR improvement results both from the coil's lower temperature and increased Q-factor (Eqs. (1) and (2)) and is in practice reduced by the preamplifier's noise factor. Neglecting preamplifier noise, Eqs. (1) and (2) can be combined to show that the expected SNR improvement is:

$$\frac{SNR_{77}}{SNR_{300}} = \sqrt{\frac{Q_{77}300\ \mathrm{K}}{Q_{300}77\ \mathrm{K}}} \tag{18}$$

where SNR_{77}, SNR_{300}, Q_{77} and Q_{300} are the coil's SNR and un-damped Q-factors at these temperatures. Using the working Q-factors for the coil mounted in the cryostat of 425 (at 300 K) and 1022 (at 77 K), respectively, Eq. (18) predicts an improvement factor of 3.1. However, when additional noise from the preamplifier is included this reduces to 3.0, in good agreement with the measured value.

Fig. 13. Coronal spin echo image of hand acquired at 0.01 T with the litz receive coil at 77 K (imaging parameters as for Fig. 12 except TR = 400 ms).

The existing theory [15,18] has been combined with estimates of dielectric losses, deduced from measurements at the self-resonance, to simulate the frequency-dependent Q-factors of pancake coils wound from solid and litz wire at room temperature and 77 K. There is general agreement between the frequency dependences of simulated and measured Q-factors for both coil types and temperatures, and particularly good agreement for the litz coil at 77 K (Fig. 8(b)). Solid coils are shown to give higher Q-factors above a few MHz but, for cooled operation below 1 MHz, litz wire coils with the correct strand diameter are better. The results in Fig. 8 illustrate that there is an optimum frequency range for each particular litz wire that depends on the number, diameter and temperature-dependent resistivity of the strands. Our surface coil used commercially available litz wire and was optimised for use at 425 kHz and 77 K, but there is scope for further work on the optimisation of litz coils for other frequencies and temperatures.

The cooled litz coil has been used to image a hand at 0.01 T with a total imaging time of 14 min. The same SNR could have been achieved without cooling the coil by additional averaging, but this would have taken 2 h 6 min.

Acknowledgments

Authors thank the University of Aberdeen for providing Frank Resmer's studentship and the Clerk Maxwell Cancer Research Fund for their financial support. Authors also thank Mr. Edward Stevenson and Mr. Peter Frew from the Bio-Medical Physics mechanical workshop for their help with numerous parts of this project.

References

[1] D.I. Hoult, P.C. Lauterbur, The sensitivity of the zeugmatographic experiment involving human samples, J. Magn. Reson. 34 (1979) 425–433.
[2] S.H. Koenig, R.D. Brown, D. Adams, D. Emerson, C.G. Harrison, Magnetic field dependence of $1/T_1$ of protons in tissue, Invest. Radiol. 19 (1984) 76–81.
[3] M.D. Harpen, Sample noise with circular surface coils, Med. Phys. 14 (1987) 616–618.

[4] A.S. Hall, B. Barnard, P. McArthur, D.J. Gilderdale, I.R. Young, G.M. Bydder, Investigation of a whole-body receiver coil operating at liquid nitrogen temperatures, Magn. Reson. Med. 7 (1988) 230–235.
[5] A.S. Hall, N.McN. Alford, T.W. Button, D.J. Gilderdale, K.A. Gehring, I.R. Young, Use of high temperature superconductor in a receiver coil for magnetic resonance imaging, Magn. Reson. Med. 20 (1991) 340–343.
[6] R.D. Black, T.A. Early, P.B. Roemer, O.M. Mueller, A. Mogro-Campero, L.G. Turner, G.A. Johnson, A high-temperature superconducting receiver for nuclear magnetic resonance microscopy, Science 259 (1993) 793–795.
[7] R.S. Withers, G.C. Liang, B.F. Cole, M. Johansson, Thin-film HTS probe for magnetic-resonance imaging, IEEE Trans. Appl. Supercond. 3 (1993) 2450–2453.
[8] J.G. van Heteren, T.W. James, L.C. Bourne, Thin film high temperature superconducting RF coils for low field MRI, Magn. Reson. Med. 32 (1994) 396–400.
[9] M. Vester, F. Steinmeyer, B. Roas, G. Thummes, K. Klundt, High temperature superconducting surface coils with liquid nitrogen or pulse tube refrigeration, in: Proc. 5th ISMRM, Vancouver, Canada, 1997, p. 1528.
[10] M.C. Cheng, B.P. Yan, K.H. Lee, Q.Y. Ma, E.S. Yang, A high temperature superconductor tape RF receiver coil for a low field magnetic resonance-imaging system, Supercond. Sci. Technol. 18 (2005) 1100–1105.
[11] J.C. Ginefri, M. Poirier-Quinot, O. Girard, L. Darrasse, Technical aspects: development, manufacture and installation of a cryo-cooled HTS coil system for high-resolution in-vivo imaging of the mouse at 1.5 T, Methods 43 (2007) 54–67.
[12] M.K. Savelainen, Magnetic resonance imaging at 0.02 T: design and evaluation of radio frequency coils with wave winding, Ph.D. Thesis, Helsinki University of Technology, 1988.
[13] G. Scott, S. Connoly, P. Morgan, A. Macovski, Body noise feasibility limits of PMRI, in: Proc. 2nd SMR, San Francisco, USA, 1994, p. 1083.
[14] H. Konijnenburg, T. Claasen-Vujcic, Overhauser imaging: requirements, design, specification and verification, Ph.D. Thesis, Technische Universiteit Delft, 1998, p. 208.
[15] F.E. Terman, Radio Engineers' Handbook, McGraw-Hill, 1943.
[16] D.I. Hoult, R.E. Richards, The signal-to-noise ratio of the nuclear magnetic resonance experiment, J. Magn. Reson. 24 (1976) 71–85.
[17] G.K. White, Experimental Techniques in Low-Temperature Physics, third ed., Clarendon, 1979.
[18] S. Butterworth, Effective resistance of inductance coils at radio frequencies, Exp. Wireless Wireless Eng. 3 (1926) 203. 302, 417, 483.
[19] J.M.S. Hutchison, W.A. Edelstein, G. Johnson, A whole-body NMR imaging machine, J. Phys. E: Sci. Instrum. 13 (1980) 947–955.
[20] H.M. Borsboom, T. Claasen-Vujcic, A.F. Mehlkopf, Measurements on bandwidth enlargement for imaging at very low fields, in: Proc. 4th SMR, New York, 1996, p. 128.
[21] G. Scott, S. Conolly, A. Macovski, Low field preamp matching design for high Q receiver coils, in: Proc. 4th SMR, New York, 1996, p. 396.
[22] P.B. Roemer, W.A. Edelstein, C.E. Hayes, S.P. Souza, O.M. Mueller, The NMR phased array, Magn. Reson. Med. 16 (1990) 192–225.
[23] C.D. Motchenbacher, F.C. Fitchen, Low-Noise Electronic Design, Wiley, 1973.
[24] D.I. Hoult, Fast recovery, high sensitivity NMR probe and preamplifier for low frequencies, Rev. Sci. Instrum. 50 (1997) 193–200.
[25] Elektrisola, Reichshof-Eckenhagen/Germany. <http://www.electrisola.de>.
[26] J309 Datasheet, Rev. G, Fairchild Semiconductor, 1997.
[27] R.M. Henkelman, Measurement of signal intensities in the presence of noise in MR images, Med. Phys. 12 (1985) 232–233.